Aeroelastic behaviour of a wing including geometric nonlinearities

M. Y. Harmin
m.harmin@liverpool.ac.uk
University of Liverpool
Liverpool, UK

J. E. Cooper
j.e.cooper@liverpool.ac.uk

ABSTRACT

A procedure for developing efficient aeroelastic reduced order models (ROMs) for aerospace structures containing geometric nonlinearities is described. The structural modelling is based upon a combined modal/FE approach that describes the non-linear stiffening effects from results of non-linear static analyses for a range of prescribed inputs. Once the structural ROM has been defined, it is coupled to the rational fraction approximation of the doublet lattice aerodynamic model corresponding to the wing planform. The aeroelastic model can then be used to predict the dynamic aeroelastic behaviour of the defined structure. The methodology is demonstrated on the aeroelastic model of a flexible high aspect ratio wing with the static deflections, LCO behaviour and gust response being predicted.

NOMENCLATURE

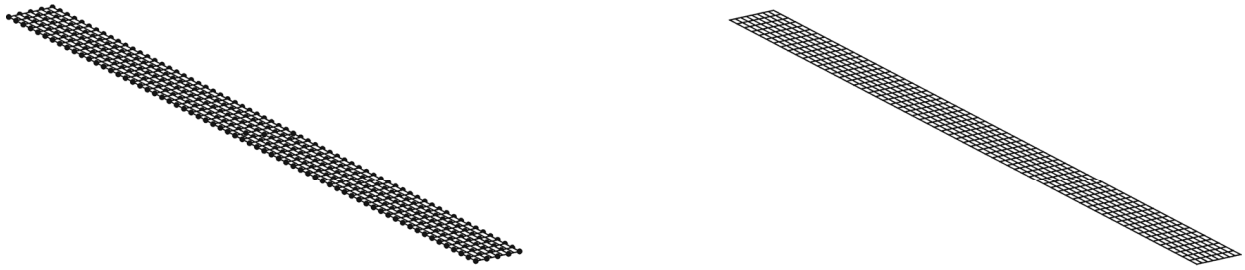
$\mathcal{A}$,$\mathcal{E}$	structural physical mass/stiffness
A,**E**	structural modal mass/stiffness
$\mathcal{A}_r$	nonlinear stiffness coefficients
AIC	aerodynamic influence matrix
$\mathcal{A}_m$	Roger aerodynamic matrices
$\mathbb{F}$	physical force vector
L	lift
M	pitching moment
$M_{\dot{\theta}}$	non-dimensional oscillatory pitch rate derivative
N	number of DOF in FE model
NA	number of nonlinear stiffness coefficients
N_L	number of aerodynamic lag parameters
NR	number of DOF in reduced modal model
NT	number of nonlinear static test cases
V	velocity
a_w	lift curve slope
b	semi-chord
c	chord
f	modal force vector
k	reduced frequency
r	physical displacement vector
p	modal displacement vector
q	dynamic pressure
s	semi wing span
β_n	aerodynamic lag parameters
ρ	air density
$\boldsymbol{\phi}$	Eigenvectors/mode shapes

1.0 INTRODUCTION

There has been a growth of interest in the development of highly flexible unmanned aerial vehicle (UAV) aircraft. Perhaps the best known instance is the Helios aircraft that failed during a flight in 2003 due to a severe gust encounter. One of the causes of the accident found by the investigation that followed was the lack of appropriate analyses for highly flexible aerospace structures[1] leading to inappropriate decisions to fly at certain flight conditions. One characteristic of such aircraft is that the structural stiffness behaves in a non-linear manner due to geometric stiffening or softening, and consequently the conventional approach to aeroelastic analysis is not valid. The geometric non-linear effects of such large structures can also have a dramatic effect upon the flight dynamics; Palacios *et al*[2] reviewed the most important aspects of high aspect ratio aircraft affected by geometric structural nonlinearities,

Paper No. 3718. Manuscript received 12 May 2011, revised version received 6 September 2011, accepted 7 October 2011.
This paper is based on a presentation given at the 2010 RAeS 2nd Aircraft Structural Design Conference, London, UK.

https://doi.org/10.1017/S0001924000006515 Published online by Cambridge University Press



(a) Structural Mesh (b) Aerodynamic Grid

Figure 1. Structural mesh and aerodynamic grid for the HALE wing.

including longitudinal stability, body-freedom flutter and gust response (and subsequent loads). They emphasised the need for computationally efficient reduced order time domain simulations to predict the coupled aeroelastic/flight dynamic interactions. The effect of geometric non-linearities is not solely confined to HALE (high altitude long endurance) aircraft, and the current generation of large commercial and military aircraft exhibit some of the above characteristics. Although there has been a great deal of research devoted to the effect of nonlinearities on aeroelastic behaviour, this has primarily been directed towards aerodynamic nonlinearities in the transonic flight regime, or discrete structural nonlinearities such as freeplay and hysteresis occurring on control surfaces. Most of the work[2-9] directed at modelling the geometric stiffening characteristics for aeroelastic models of HALE type aircraft has employed equivalent non-linear beam models.

There have been a number of approaches developed to use commercial finite element software to enable the development of reduced order structural models. In particular the modal/FE (MFE) approach of McEwan *et al*[10-11] performs a static analysis for a number of prescribed static loading cases. These displacements are then curve fitted using a regression analysis in order to define non-linear stiffness terms that can be added to the conventional modal model. A similar approach is used in the ELSTEP methodology[12-13] which applies prescribed displacements. Once the reduced order model is produced, it is then very efficient to run time domain simulations for a large number of design cases. The MFE approach has been used very successfully[10,14] for the prediction of response of aircraft panels subjected to large acoustic excitations. A recent application of the ELSTEP approach has been to combine it [15,16] to hypersonic aerodynamic models in order to produce efficient coupled non-linear aeroelastic models of membrane type structures.

In this paper, the MFE approach of McEwan *et al*[10,11] is implemented to model the geometric nonlinearities of the Patil and Hodges HALE wing model[4-6]. The prescribed load cases and resultant displacements from the static nonlinear test cases are transformed into modal coordinates using the modal transformation of the underlying linear system. A regression analysis is then performed to curve-fit the sets of nonlinear stiffness force/displacement maps in order to find the unknown nonlinear modal stiffness coefficients. Having obtained the nonlinear modal model, a time domain aeroelastic analysis was performed by coupling the structural model with the rational function approximation (RFA) of doublet lattice aerodynamics using the Roger method. It is shown how this approach can predict the static deflection, gust response and limit cycle oscillation (LCO) behaviour of the nonlinear wing; however, it is also shown that care needs taken in choosing the modes that are considered in the analysis. Finally, the effect of varying different structural parameters on the nonlinear aeroelastic behaviour is investigated.

2.0 SIMULATION MODEL

The Patil and Hodges wing model[4-6] was used to illustrate the methodology. Figure 1 shows the NASTRAN finite element representation of the structural and aerodynamic grids and the properties are shown in Table 1. The wing was modelled as a simple flat plate using shell elements (PSHELL), and a fully clamped boundary condition was defined at the root of the wing. A mesh convergence study was made to determine the appropriate number of elements to be included in the model in order to give a reasonable accuracy to the overall solution.

Linear static and normal mode analyses were first performed to obtain the linear behaviour of the model, from which the mass and stiffness matrices in both physical and modal co-ordinates were determined. Figure 2 shows the spatial distribution of the first five mode shapes; note that there are three bending modes, a chordwise bending mode, and a torsion mode. Flutter analysis was carried out to predict the flutter speed at the given flight condition by using the well known *P-K* method [17].

A nonlinear static analysis was then performed, and Fig. 3 demonstrates clearly that the structure experiences a stiffness hardening effect, occurring as the tip of the wing is deflected above 2·5m.

3.0 MATHEMATICAL MODELS

3.1 Combined modal/finite element approach[10,11]

The underlying theme of this work is the application of the MFE for highly flexible aeroelastic systems. This section describes the generation of the nonlinear structural model using the approach.

Table 1
Patil-Hodges wing data[4-6]

Half span	b	16m
Chord	c	1m
Mass per unit length	m/b	0·75kg/m
Moment of inertia (50% chord)	δI_{zz}	0·063kg/m
Spanwise elastic axis		50% chord
Centre of gravity		50% chord
Bending rigidity	EI_{xx}	2×10^4 Nm^2
Torsional rigidity	GJ	$0{\cdot}636 \times 10^4$ Nm^2
Bending rigidity (edgewise)	EI_{yy}	4×10^6 Nm^2

https://doi.org/10.1017/S0001924000006515 Published online by Cambridge University Press

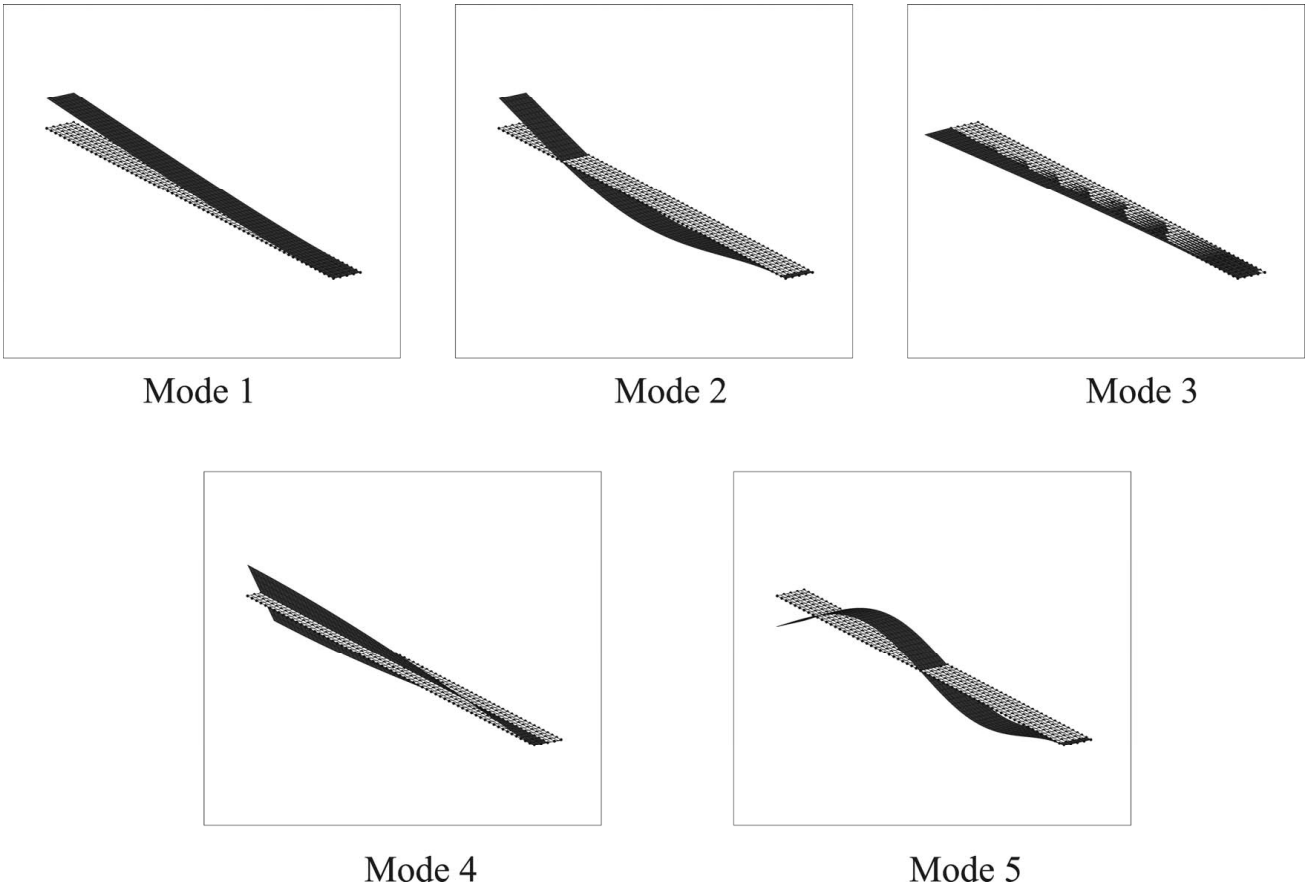


Figure 2. First five bending mode shapes of baseline undeflected model.

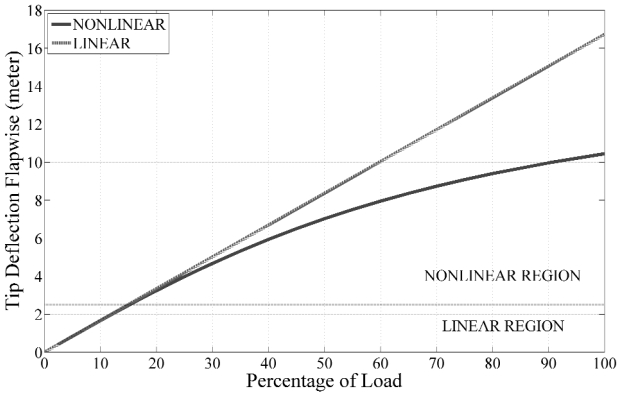


Figure 3. Wing tip deflection for applied loads – linear and nonlinear static analysis.

3.1.1 Nonlinear structure modal model

The equations of motion of dynamic system in physical space including stiffness nonlinearity can be represented as

$$\mathbb{A}\ddot{\boldsymbol{r}} + \alpha\mathbb{A}\dot{\boldsymbol{r}} + \mathbb{E}_L(\boldsymbol{r}) + \{\mathbb{E}_{NL}(\boldsymbol{r})\} = \{\mathbb{F}\} \quad \ldots (1)$$

where $\mathbb{A}$ is the $N \times N$ assembled mass matrix, $\mathbb{E}_L$ is the $N \times N$ assembled linear stiffness matrix, $\mathbb{E}_{NL}(\boldsymbol{r})$ is the $N \times 1$ vector of nonlinear stiffness function, $\mathbb{F}$ is the $N \times 1$ vector of applied nodal forces, α is the proportional mass damping coefficient, and $\mathbf{r}(\mathbf{t})$ is the $N \times 1$ vector of spatial displacements. The transformation between the physical space and modal space is performed using the modal transformation

$$\mathbf{r(x,t)} = \boldsymbol{\phi}\mathbf{(x)p(t)} \quad \ldots (2)$$

where $\mathbf{p}(\mathbf{t})$ is the $NR \times 1$ vector of time-dependent generalised modal co-ordinates and $\boldsymbol{\phi}(\mathbf{x})$ is the $N \times NR$ matrix of the underlying linear mode shapes. The number of degrees of freedom in the modal model (NR) can be reduced ($NR \ll N$) depending on the frequency range or modes of interest. Substituting the modal transformation of equation (2) into Equation (1) and pre-multiplying by $[\boldsymbol{\phi}]^{\mathbf{T}}$ yields

$$\boldsymbol{\phi}^{\mathbf{T}}\mathbb{A}\boldsymbol{\phi}\ddot{\mathbf{p}} + \alpha\boldsymbol{\phi}^{\mathbf{T}}\mathbb{A}\boldsymbol{\phi}\dot{\mathbf{p}} + \boldsymbol{\phi}^{\mathbf{T}}\mathbb{E}_{\mathbf{L}}\boldsymbol{\phi}\mathbf{p} + \boldsymbol{\phi}^{\mathbf{T}}\{\mathbb{E}_{\mathbf{NL}}(\mathbf{r})\}\boldsymbol{\phi}\mathbf{p} = \boldsymbol{\phi}^{\mathbf{T}}\{\mathbb{F}\} \quad \ldots (3)$$

Here, a set of coupled physical systems are modified into a set of uncoupled single DOF modal systems by using the orthogonality of the modes. Therefore, the equations of motion in modal co-ordinates become

$$\mathbf{A}\ddot{\mathbf{p}} + \alpha\mathbf{A}\dot{\mathbf{p}} + \mathbf{E}_{\mathbf{L}}\mathbf{p} + \{\mathbf{E}_{\mathbf{NL}}(\mathbf{p})\} = \{\mathbf{f}\} \quad \ldots (4)$$

where matrix $\mathbf{A}$ and $\mathbf{E}_{\mathbf{L}}$ are now diagonal matrices of size $NR \times NR$. However, it should be noted that the nonlinear modal stiffness matrix $\{\mathbf{E}_{\mathbf{NL}}(\mathbf{p})\}$ which is a $NR \times 1$ vector, may contain cross-coupling terms and is a function of modal co-ordinate, $\mathbf{p}(t)$.

https://doi.org/10.1017/S0001924000006515 Published online by Cambridge University Press

3.1.2 Nonlinear static test cases

The implementation of the combined modal/finite element (FE) approach is based on nodal deflections obtained from a number of prescribed static non-linear load cases. Thus, when a static system is considered, the equations of motion which are given by Equation (4) reduce to

$$\mathbf{E_L p} + \{\mathbf{E_{NL}(p)}\} = \{\mathbf{f}\} \quad \ldots (5)$$

and by rearranging the above equation, the nonlinear stiffness restoring forces can be written as

$$\{\mathbf{f}\} - \mathbf{E_L p} = \{\mathbf{E_{NL}(p)}\} \quad \ldots (6)$$

A set of finite element nonlinear static test cases have to be defined by prescribing a set of applied loads in the finite element nodal space. The nonlinear modal stiffness coefficients are identified by performing regression analysis on sets of information obtained from several nonlinear static test cases which have been transformed into the modal co-ordinates. In this work, the load cases are defined based upon the single mode profile which was generated using the equation

$$\{\mathbb{F}\} = \boldsymbol{a_r}\left(\frac{2\boldsymbol{i}}{\boldsymbol{g}-1} - 1\right)\{\boldsymbol{\phi}\}_{\boldsymbol{r}} \quad \ldots (7)$$
$$i = 0,1,..\ g-1$$

where a_r are the scalar weighting factors. These weighting factors determine the contribution of each mode used for the various mode profiles. A grid density g is used to define intermediate test loads in order to have a wide range of sampling space. Care has to be taken when defining these parameters so that the selected test cases are able to cover all the possible behaviour within the desired deflection ranges.

For the analysis based upon the undeformed straight wing, the chordwise bending mode can be safely neglected as it has no impact on the calculation of aerodynamic loads that couple with the structural modes. This assumption only holds true for the case of pure edgewise bending. Due to the unknown characteristics of the stiffness nonlinearities, it has to be assumed that the nonlinear cross-couplings between the bending modes have significant effect on overall static and dynamic responses.

The transformation of nodal displacement into modal space is calculated from the solution of

$$\boldsymbol{\phi p} = \boldsymbol{r} \quad \ldots (8)$$

while the applied modal force vector is obtained as

$$\boldsymbol{f} = \boldsymbol{\phi}^T \mathbb{F} \quad \ldots (9)$$

3.1.3 Regression analysis

An ordinary polynomial approach has been used to curve fit the nonlinear force/displacement relationship. Simultaneous coupling of up to two modes was considered as other studies made by the authors have found that the simultaneous couplings of more than two modes of this structure are very weak and can be safely neglected. The polynomial expression of the nonlinear restoring forces was derived as the following series of up to third order for some mode r

$$\mathbf{E_{NL}}_{(r)}\ (p_1, p_2, p_{NR}) = \sum_{s=1}^{NR}\sum_{i=2}^{3} \mathcal{A}_r p_s^i + \sum_{s=1}^{NR-1}\sum_{s+1}^{NR}\sum_{i=1}^{2}\sum_{j=1}^{3-i} \mathcal{A}_r = p_s^i p_t^j \quad \ldots (10)$$

Upon completion of the static nonlinear test cases, and with the acquired data of load-displacement in modal space, the nonlinear restoring force for each of the test cases can now be fitted to find the unknown nonlinear modal stiffness coefficients in a least squares sense. The nonlinear restoring forces for a certain mode r can now be shown in matrix form to be

$$\begin{Bmatrix} f_{r(1)} - \mathbf{E}_{L(r)} p_{r(1)} \\ f_{r(2)} - \mathbf{E}_{L(r)} p_{r(2)} \\ \vdots \\ \vdots \\ f_{r(NT)} - \mathbf{E}_{L(r)} p_{r(NT)} \end{Bmatrix} = \begin{bmatrix} p^2_{1\,(1)} & p^3_{1\,(1)} & \cdots & \cdots \\ p^2_{1\,(2)} & p^3_{1\,(2)} & \cdots & \cdots \\ \vdots & \vdots & \cdots & \cdots \\ \vdots & \vdots & \cdots & \cdots \\ p^2_{1\,(NT)} & p^3_{1\,(NT)} & \cdots & \cdots \end{bmatrix} \begin{Bmatrix} \mathcal{A}_{r(1)} \\ \mathcal{A}_{r(2)} \\ \vdots \\ \vdots \\ \mathcal{A}_{r(NA)} \end{Bmatrix} \quad \ldots (11)$$

or represented as

$$\{f_r\}_{NL} \approx \{\hat{f}_r\}_{NL} = [\mathbf{D_r}]\{\mathcal{A}_r\} \quad \ldots (12)$$

Here, $\{(\hat{fr})\}_{NL}$ is a $NT \times 1$ vector of fitted values of nonlinear modal stiffness restoring forces, $[D_r]$ is $NT \times NA$ design matrix and $\{\mathcal{A}_r\}$ is $NA \times 1$ vector containing the unknown values of nonlinear stiffness coefficients where both of these matrices were developed based on Equation (10). The singular value decomposition (SVD) technique was used to solve for the nonlinear stiffness coefficient $\{\mathsf{x}_r\}$. The backward elimination approach was used to remove those nonlinear polynomial terms that gave less significance to the overall solution[10, 11].

3.1.4 Verification

The accuracy of the estimated nonlinear reduced order modal model (NLROMM) was validated by first defining the modal force case, and the NLROMM solved using a Newton-Raphson approach in order to compute the modal displacements of the solution. The modal displacements were then transformed into physical space and comparisons made with a corresponding finite element nonlinear static analysis. Once close agreement between the NLROMM and finite element analysis (FEA) was achieved on a series of test cases, the NLROMM was considered suitable to be used for the aeroelastic analysis[18].

3.2 Dynamic aeroelastic model

The general form of the aeroelastic analysis was developed by coupling the aerodynamic panels and the FE representations of the considered model[19]. When applied to dynamic systems, the dynamic behaviour of FE model relates the displacement and acceleration vectors to the force vector via the overall stiffness and mass matrices such that

$$\mathbf{R} = \mathcal{A}\ddot{\mathbf{r}} + \mathbb{E}\mathbf{r} \quad \ldots (13)$$

This equation will be coupled with the aerodynamic model of lift L and pitching moment M to form the dynamic aeroelastic equations as

$$\mathcal{A}\ddot{\mathbf{r}} + \mathbb{E}r = L + M \quad \ldots (14)$$

3.2.1 Inclusion of frequency dependent aerodynamics

An aerodynamic model derived from the doublet lattice method (DLM) was considered throughout this work in order to predict accurately the dependency of aerodynamic forces and moments on the frequency content of dynamic motions[19]. From Equation (14), the full aeroelastic equation with frequency dependent aerodynamics may be written as

$$\mathcal{A}\ddot{\mathbf{r}} + \mathbb{E}\mathbf{r} = \frac{\rho V}{2}\frac{b}{k}\mathbf{AIC_i r} + \frac{\rho V^2}{2}\mathbf{AIC_{ir}} \quad \ldots (15)$$

where the AIC matrices are a function of the reduced frequency

https://doi.org/10.1017/S0001924000006515 Published online by Cambridge University Press

$$k = \frac{\omega b}{V} \quad \ldots (16)$$

and the subscripts refer to the real and imaginary parts. The modal aeroelastic equations of motion with the inclusion of geometric nonlinearities can then be expressed as

$$\mathbf{A}\ddot{\mathbf{p}} + \mathbf{E}_{\mathbf{L}}\mathbf{p} + \mathbf{E}_{\mathbf{NL}}(\mathbf{p}) = \frac{\rho V}{2}\frac{b}{k}\phi^{I}\mathbf{AIC}_{\mathbf{i}}\phi\dot{\mathbf{p}} + \frac{\rho V^2}{2}\mathbf{AIC}_{\mathbf{r}}\phi^{t}\{\mathbf{p} + \mathbf{p_0}\} = \mathbf{Q}_{\mathbf{aero}} \quad \ldots (17)$$

where $\mathbf{Q}_{\mathbf{aero}}$ are the generalised aerodynamic force.

The AICs were extracted from the MSC NASTRAN aeroelastic analysis using the direct matrix abstraction program (DMAP) over a range of reduced frequencies for given flight conditions. The Roger procedure[20] was then used to determine the rational fraction approximation (RFA) of the AIC matrices and then a state-space time domain model may be formed. With this approach, the use of convolution time domain integrals can be avoided. This mathematical representation can be solved using time domain integration and now inclusion of nonlinear terms is feasible.

The above equation can be transformed and written in the Laplace domain as

$$\left(\mathbf{A}s^2 + \mathbf{E}_{\mathbf{L}}\right)\mathbf{p}(s) + \mathbf{E}_{\mathbf{NL}}(\mathbf{p}(s)) = \frac{\rho V^2}{2}\mathbf{Q}(s)\mathbf{p}(s) \quad \ldots (18)$$

and the RFA of the generalised aerodynamic matrices $\mathbf{Q}(s)$ are written in the form

$$\mathbf{Q}(s) = \mathbf{A}_0 + \mathbf{A}_1\left(\frac{sb}{V}\right) + \mathbf{A}_2\left(\frac{sb}{V}\right)^2 + \left(\frac{V}{b}\right)\sum_{n=1}^{NL}\frac{\mathbf{A}_{\mathbf{n+2}}s}{s + \left(\frac{V}{b}\right)\beta_{\mathbf{n}}} \quad \ldots (19)$$

Here, $\mathbf{A}_{\mathbf{n}}$ is a $NR \times NR$ unknown matrix to be found and $\boldsymbol{\beta}_{\mathbf{n}}$ are the aerodynamic lag parameters which can be calculated as[20]

$$\beta_i = -\frac{1 \cdot 7 k_{max} i}{\left(N_L + 1\right)^2} \quad \ldots (20)$$

where k_{max} is the maximum reduced frequency at which the AIC matrices were obtained and N_L is the number of lag parameters. Recalling the definition of the reduced frequency, and since the Laplace variable $s = i\omega$, the RFA of Equation (19) can be written in terms of reduced frequency as

$$\mathbf{Q}(s) = \mathbf{A}_0 + \mathbf{A}_1(ik) + \mathbf{A}_2(ik)^2 + \sum_{n=1}^{N_L}\frac{\mathbf{A}_{\mathbf{n+z}}ik}{(ik + \beta_n)} \quad \ldots (21)$$

The unknown A_n coefficients can be estimated using least squares to compare the sum of squares errors between the RFA and AIC matrix[19,20]. Having estimated the unknown A_{rs} values, the time domain model becomes

$$\mathbf{A}\ddot{\mathbf{p}} + \mathbf{E}_{\mathbf{L}}\mathbf{p} + \mathbf{E}_{\mathbf{NL}}(\mathbf{p}) = \mathbf{A}_0 q\mathbf{p} + \left(\frac{b}{V}\right)\mathbf{A}_1 q\dot{\mathbf{p}} + \left(\frac{b}{V}\right)^2\mathbf{A}_z q\ddot{\mathbf{p}} + q\sum_{n=1}^{N_L}\mathbf{A}_{\mathbf{n}}\dot{\mathbf{p}}_{\mathbf{a_n}} \quad \ldots (22)$$

where $q = \frac{\rho V^2}{2}$ is the dynamic pressure. Rearranging the above expression yields

$$\left(\mathbf{A} - \left(\frac{b}{V}\right)^2\mathbf{A}_2 q\right)\ddot{\mathbf{p}} - \left(\frac{b}{V}\right)\mathbf{A}_1 q\dot{\mathbf{p}} + \left(\mathbf{E}_{\mathbf{L}} - \mathbf{A}_0 q\right)\mathbf{p} = -\mathbf{E}_{\mathbf{NL}}(\mathbf{p}) + q\sum_{n=1}^{N_L}\mathbf{A}_{\mathbf{n}}\dot{\mathbf{p}}_{\mathbf{a_n}} \quad \ldots (23)$$

or in a shorthand notation

$$\left(\tilde{\mathbf{A}}\right)\ddot{\mathbf{p}} + \tilde{\mathbf{D}}\dot{\mathbf{p}} + \left(\tilde{\mathbf{E}}_{\mathbf{L}}\right)\mathbf{p} = -\mathbf{E}_{\mathbf{NL}}(\mathbf{p}) + q\sum_{\mathbf{n}=1}^{N_L}\mathbf{A}_{\mathbf{n}}\dot{\mathbf{p}}_{\mathbf{a_n}}` \quad \ldots (24)$$

The augmented states which arise from the convolution integral of the inverse Laplace transform of the $Q(s)$ matrix are defined by

$$\dot{\mathbf{p}}_{\mathbf{a_n}} = \int_0^t \dot{\mathbf{p}}e^{-\frac{V}{b}\beta_n(t-\tau)}\mathrm{d}\tau \quad 1 \le n \le N_L \qquad \ddot{\mathbf{p}}_{\mathbf{a_n}} = \dot{\mathbf{p}} - \frac{V}{b}\beta_n\dot{\mathbf{p}}_{\mathbf{a_n}} \quad \ldots (25)$$

but these are not explicitly calculated. Equations (24) and (25) can now be combined together to form the state space equations. These can be formulated by transforming these expressions to a first order differential equation with the states and the state space matrix defined as

$$\mathbf{x} = \left[\mathbf{p}^{\mathbf{T}} \quad \dot{\mathbf{p}}^{\mathbf{T}} \quad \dot{\mathbf{p}}_{\mathbf{1}}^{\mathbf{T}} \quad \dot{\mathbf{p}}_{\mathbf{2}}^{\mathbf{T}} \quad \cdots \quad \dot{\mathbf{p}}_{\mathbf{a_{N_L}}}^{\mathbf{T}}\right]^{\mathbf{T}}$$
$$\dot{\mathbf{x}} = \left[\mathbf{A}_{\mathbf{s}}\right]\{\mathbf{x}\}\{\mathbf{b}\} \quad \ldots (26)$$

where the state matrix $\mathbf{A}_{\mathbf{s}}$ is:

$$\mathbf{A}_{\mathbf{s}} = \begin{bmatrix} \mathbf{0} & \mathbf{I} & \mathbf{0} & \mathbf{0} & \mathbf{0} & \mathbf{0} \\ -\tilde{\mathbf{A}}^{-1}\tilde{\mathbf{E}} & -\tilde{\mathbf{A}}^{-1}\tilde{\mathbf{D}} & \tilde{\mathbf{A}}^{-1}\mathbf{A}_3 & \cdots & \cdots & \tilde{\mathbf{A}}^{-1}\mathbf{A}_{\mathbf{N_L-2}} \\ \mathbf{0} & \mathbf{I} & -\frac{V}{b}\beta_1\mathbf{I} & \mathbf{0} & \cdots & \mathbf{0} \\ \mathbf{0} & \mathbf{I} & \mathbf{0} & -\frac{V}{b}\beta_2\mathbf{I} & \ddots & \vdots \\ \vdots & \vdots & \vdots & \ddots & \ddots & \mathbf{0} \\ \mathbf{0} & \mathbf{I} & \mathbf{0} & \cdots & \mathbf{0} & -\frac{V}{b}\beta_{N_L}\mathbf{I} \end{bmatrix} \quad \ldots (27)$$

and the geometric nonlinear force vector is expressed as

$$\{\mathbf{b}\} = \begin{Bmatrix} \mathbf{0} \\ -\mathbf{A}^{-1}\mathbf{E}_{\mathbf{NL}}(\mathbf{P}) \\ \mathbf{0} \\ \mathbf{0} \\ \vdots \\ \mathbf{0} \end{Bmatrix} \quad \ldots (28)$$

The state space formulation can now be solved using the time domain integration to calculate the response for any given input force such as initial deflection, initial velocity or gust.

4.0 RESULTS BASED ON THE LINEAR UNDEFLECTED MODEL

Using the approach described above, with the nonlinear terms derived from application of the undeflected mode shapes, the effect of varying the flexural rigidity *EI* and torsional rigidity *GJ* was considered. Figure 4 shows the sensitivity of the linear natural frequencies with respect to *EI* and *GJ* parameters and Table 2 summarises the linear flutter-divergence results. Whereas variations in *EI* affect the bending frequencies, this has little effect upon divergence and flutter speeds, however, varying *GJ* affects the torsional frequency, and both the divergence and flutter speeds are very sensitive in *GJ*.

Consider now the effect of varying *EI* and *GJ* on the nonlinear aeroelastic model. Of particular interest is to simulate the steady state response following some initial disturbance, in order to examine the stability. Above the linear flutter speed, limit cycle oscillations (LCOs) form[19] and the amplitude grows as the speed increases beyond the critical flutter speed. Figure 5 shows how the LCO amplitudes (tip deflection and twist) are affected by *EI* and *GJ*; the LCO amplitude reduces with increasing *EI* however the onset of

https://doi.org/10.1017/S0001924000006515 Published online by Cambridge University Press

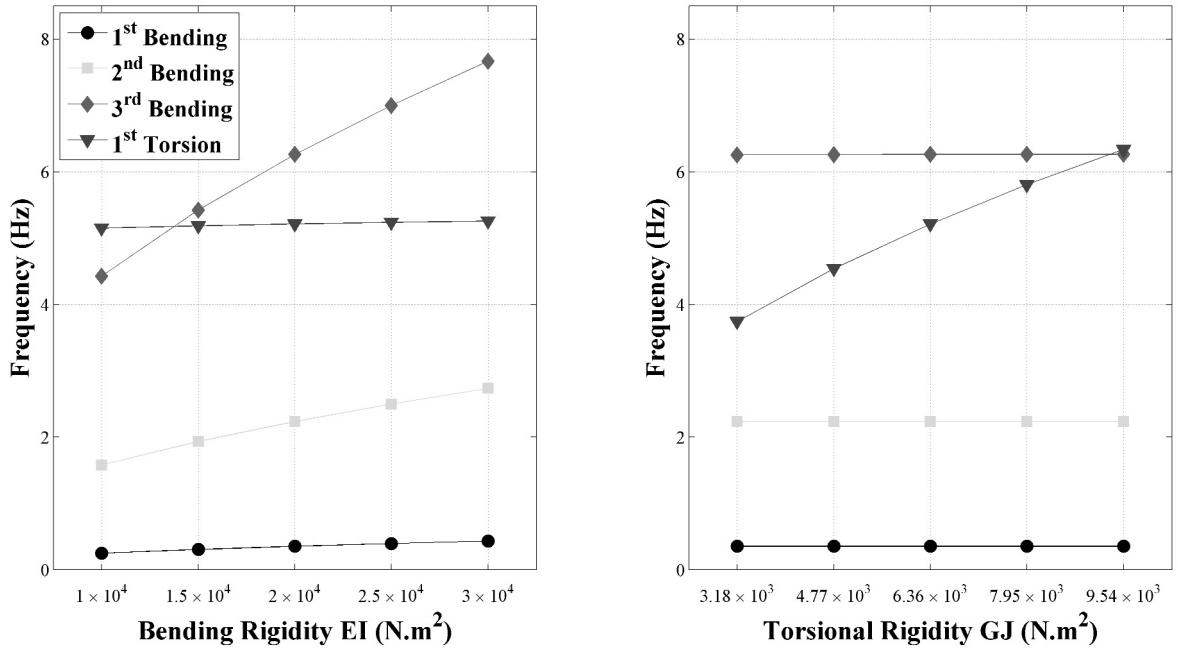


Figure 4. The sensitivities of bending modes and torsional mode frequency with respect to (a) bending rigidity, EI , (b) torsional rigidity, GJ.

Table 2
Linear aeroelastic results (flutter — divergence)

EI (Nm^2)	GJ (Nm^2)	Linear Aeroelastic Flutter (ms^{-1})	Divergence (ms^{-1})
1×10^4	$6{\cdot}36 \times 10^3$	29·59	33·10
$1{\cdot}5 \times 10^4$	$6{\cdot}36 \times 10^3$	29·70	33·30
2×10^4	$6{\cdot}36 \times 10^3$	29·78	33·50
$2{\cdot}5 \times 10^4$	$6{\cdot}36 \times 10^3$	29·83	33·65
3×10^4	$6{\cdot}36 \times 10^3$	29·88	33·80

(a)

EI (Nm^2)	GJ (Nm^2)	Linear Aeroelastic Flutter (ms^{-1})	Divergence (ms^{-1})
2×10^4	$3{\cdot}18 \times 10^3$	21·29	24·08
2×10^4	$4{\cdot}77 \times 10^3$	25·85	29·20
2×10^4	$6{\cdot}36 \times 10^3$	29·78	33·50
2×10^4	$7{\cdot}95 \times 10^3$	33·22	37·30
2×10^4	$9{\cdot}54 \times 10^3$	36·33	40·70

(b)

LCO is not affected. Conversely, the amplitude does increase with torsional stiffness, but this is more of a function of the LCO onset speed increasing, causing greater aerodynamics forces to act upon the bending motions.

Gust response analysis[21] was performed for three different '1 – Cosine' gust wavelengths. Figure 6 shows a response comparison for the linear and geometric nonlinear structure at a speed below than the linear flutter speed. For the geometric nonlinear case, the maximum tip response is much less than the linear case and this difference becomes more significant as the gust length increases. Figure 7 shows the same analysis but this time above the linear flutter speed. In all cases the same final LCO amplitude is achieved, which is primarily a torsional effect. The change in the bending deflection is due to the increasing maximum gust amplitude at greater gust lengths[19].

5.0 INFLUENCE OF DEFORMED STRUCTURE ON THE AEROELASTIC BEHAVIOUR

As the wing is very flexible, it undergoes very high deflections leading to a strong nonlinear coupling between the bending and torsion modes, including the edgewise bending mode (previously ignored)[5]. The structural and aeroelastic characteristics of the wing have to be investigated by linearising the problem about the nonlinear statically deformed shape. In this work, the deformed state was obtained by applying the uniform static forces along the wing with the vector of the forces in the direction of flapwise bending. This results in a much simpler relationship between the deformation and aeroelastic instabilities rather than obtaining the deformed state

https://doi.org/10.1017/S0001924000006515 Published online by Cambridge University Press

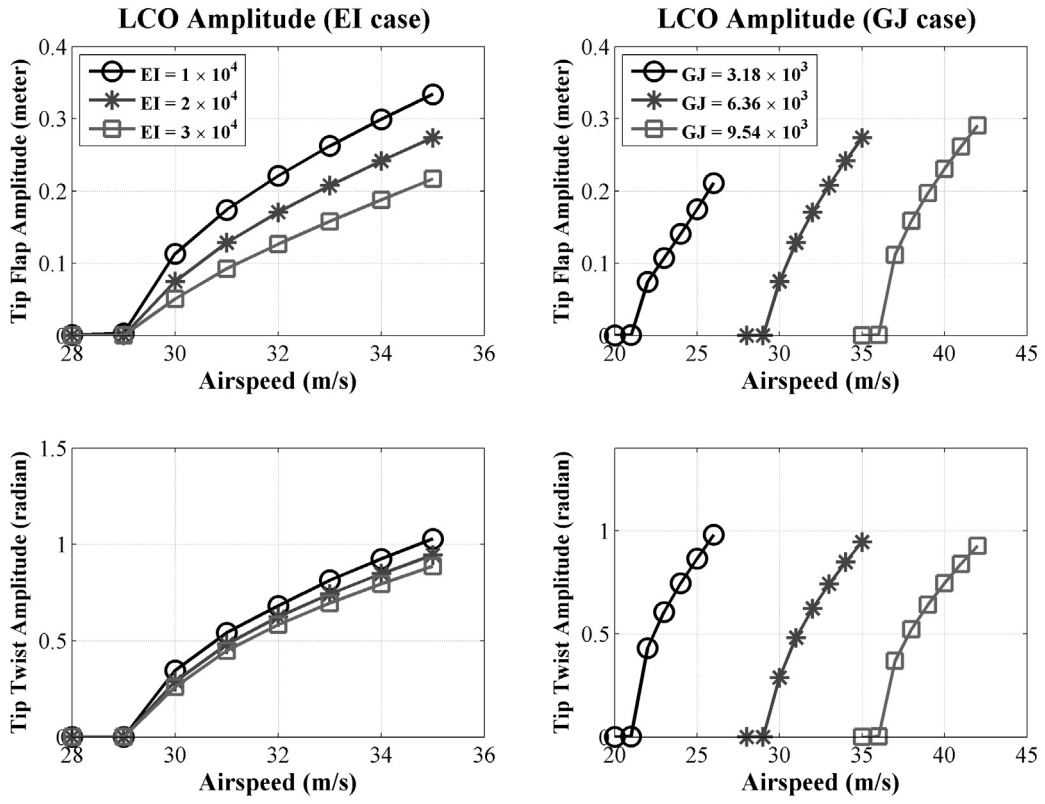


Figure 5. LCO amplitude of tip deflection and tip twist.

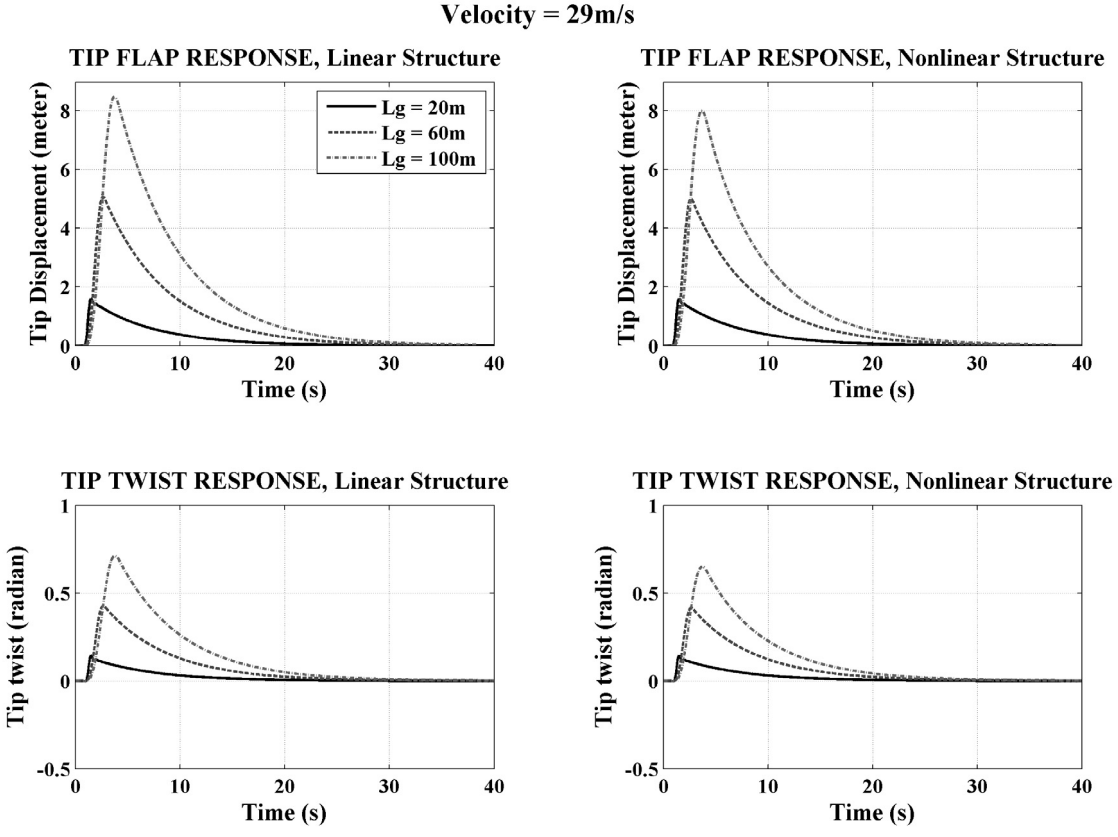


Figure 6. Time history of tip flap and tip twist response under influence of 1-Cosine gust.

https://doi.org/10.1017/S0001924000006515 Published online by Cambridge University Press

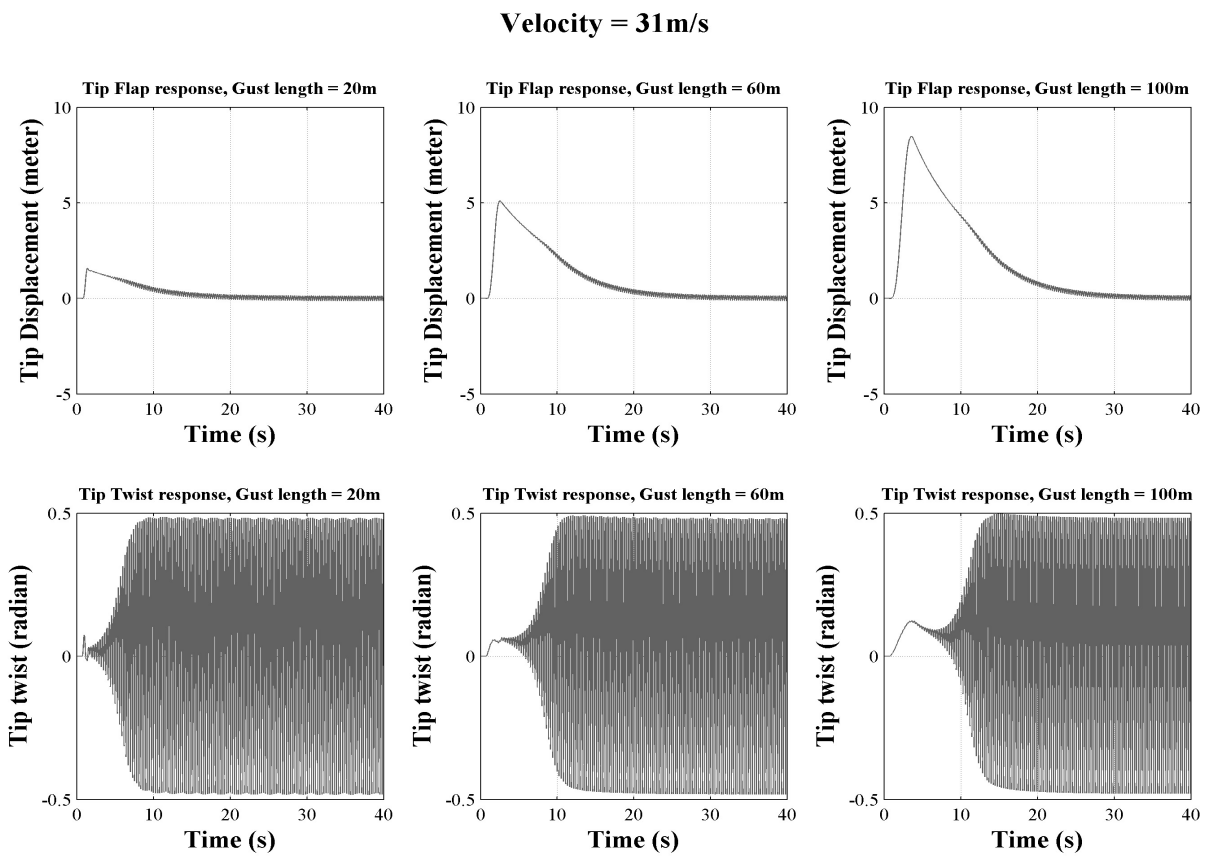


Figure 7. Time history of tip flap and tip twist response under influence of 1-Cosine gust (nonlinear case – above linear flutter speed).

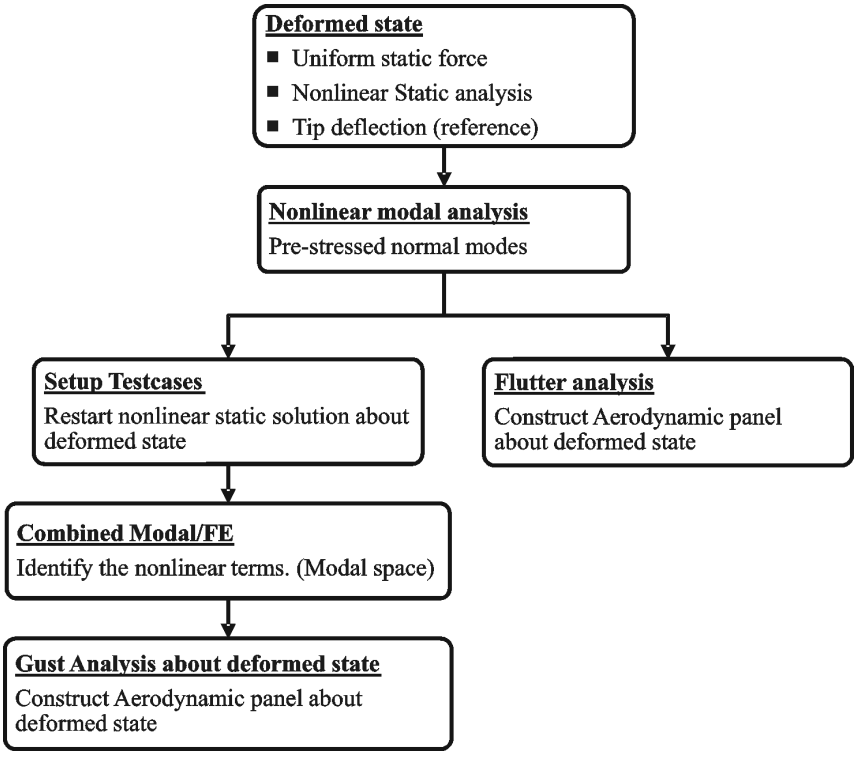


Figure 8. Analysis flow chart.

https://doi.org/10.1017/S0001924000006515 Published online by Cambridge University Press

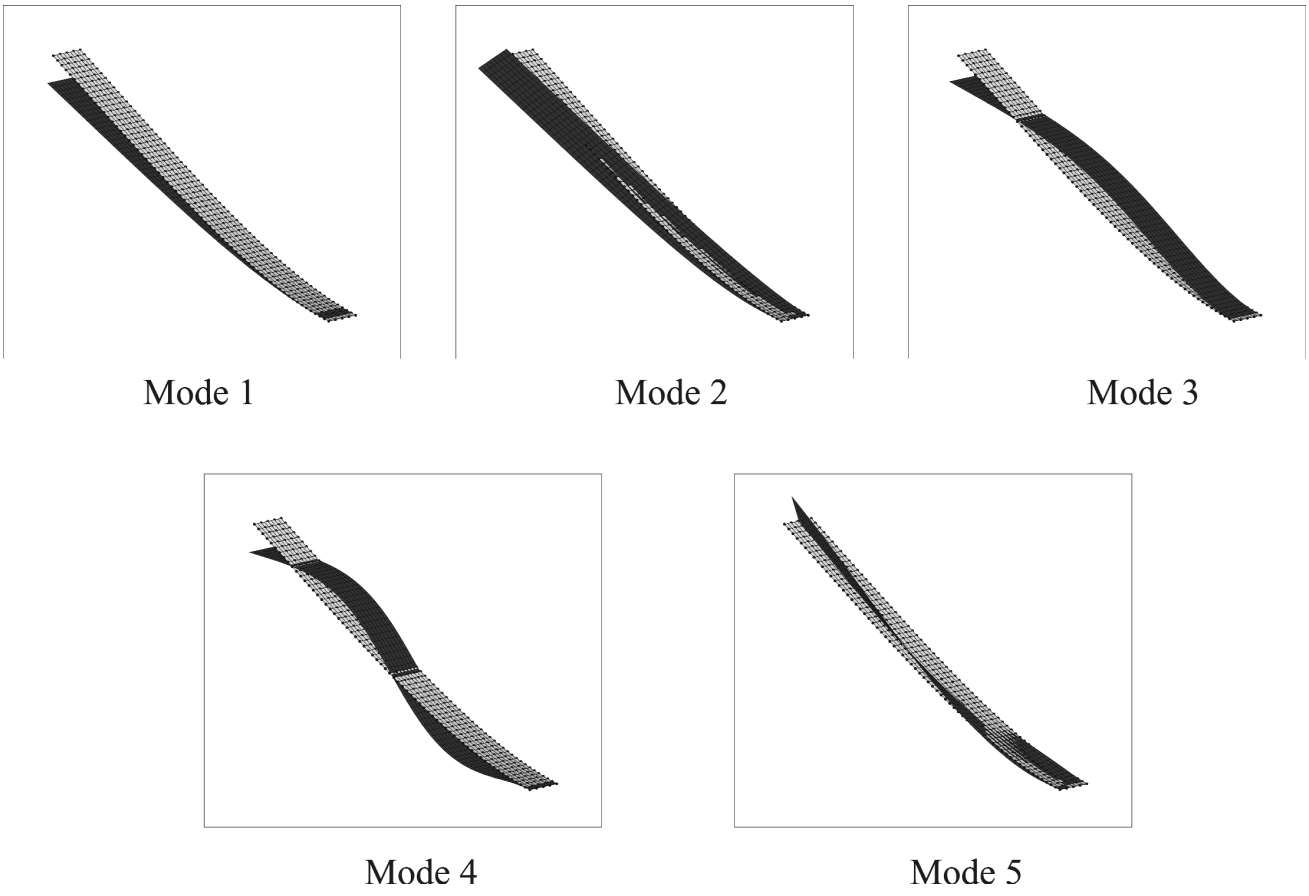


Figure 9. The first five nonlinear mode shapes of the deformed wing (tip deflection = 4metre).

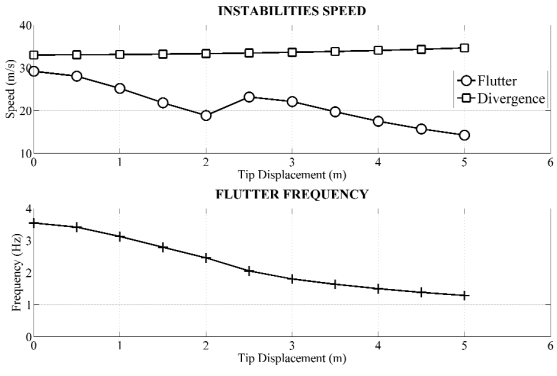


Figure 10. Variation of structural frequencies with tip displacement.

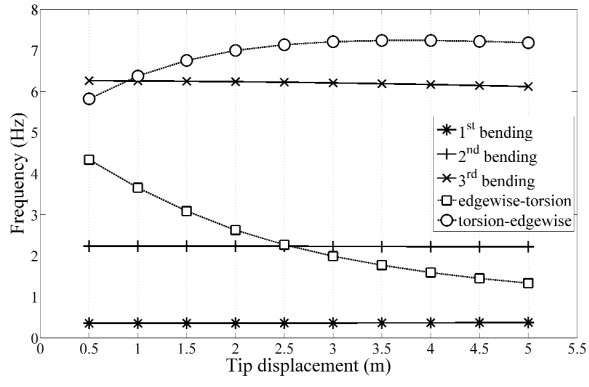


Figure 11. Correlation of aeroelastic instabilities and wing tip displacement.

via a trim angle-of-attack[5,6]. The nonlinear eigensolution of the structural analysis were obtained using MSC NASTRAN nonlinear modal analysis which is computed based upon the updated stiffness about a nonlinear statically deformed state. The deformed coordinates and the structural eigensolution are then assigned to the ZAERO package for the aeroelastic calculation. A basic flowchart of the analysis is shown in Fig. 8

Figure 9 illustrates the first five mode shapes of the deformed structure at some static deflection. It is shown clearly that the nonlinear normal modes of the curved wing now include a coupling between the torsion and edgewise bending modes. Therefore all of the five modes are of relevance for the aeroelastic computation and were included in the following computations.

Figure 10 shows the relationship between the structural

https://doi.org/10.1017/S0001924000006515 Published online by Cambridge University Press

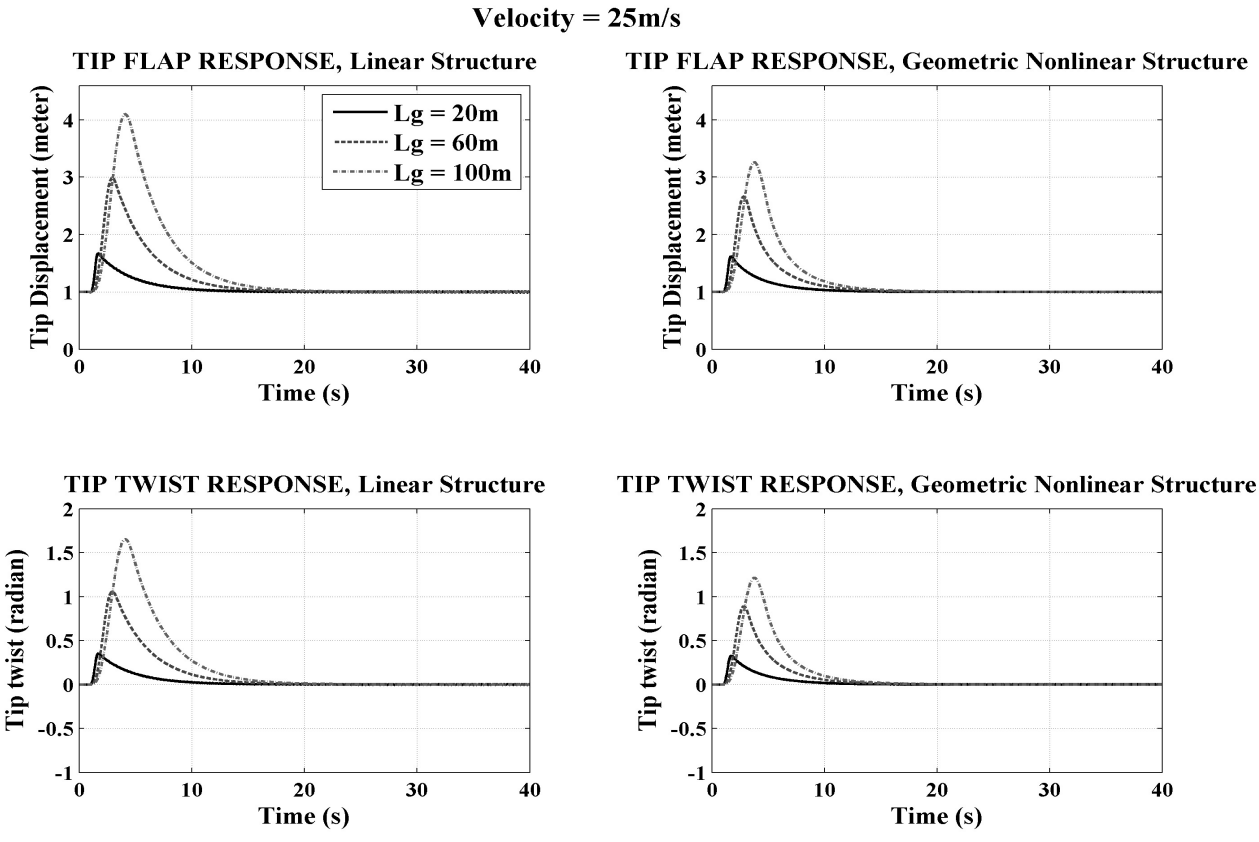


Figure 12. Time history of tip flap and tip twist response under influence of 1-Cosine gust (Linear and nonlinear case) – deformed case.

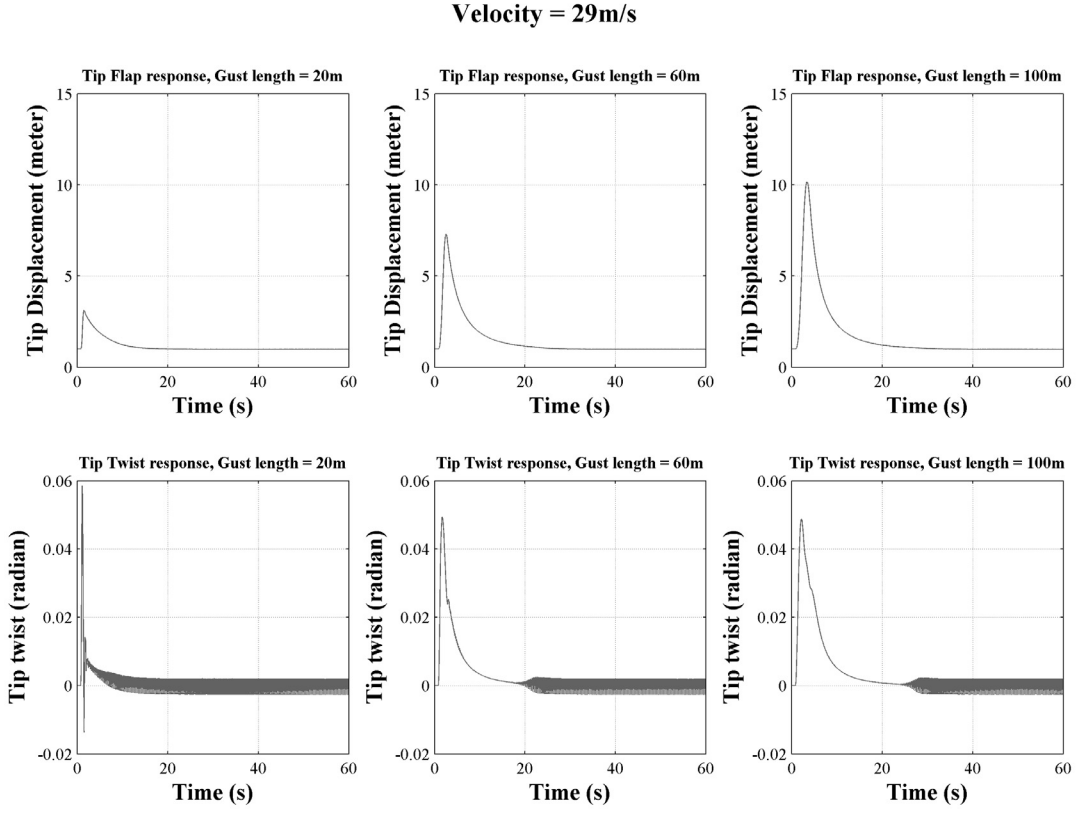


Figure 13. Time history of tip flap and tip twist response under influence of 1-Cosine gust (nonlinear case – above linear flutter speed) – deformed case.

https://doi.org/10.1017/S0001924000006515 Published online by Cambridge University Press

frequencies and the tip deflections. The edgewise-torsion frequency decreases with higher tip deflection, whereas the torsion-edgewise frequency increases to some constant value. The flapwise bending frequencies are unaffected. Figure 11 presents the effect of the tip deflection on aeroelastic instabilities. The flutter speed is shown to be very sensitive to the static wing deformation. From the investigation of the measured eigensolution of aeroelastic system of the deformed wing, flutter occurs mainly due to the interaction between the edgewise-torsion mode and the flapwise modes. At a larger scale of wing tip deflection, the edgewise-torsion frequency continues to decrease and this leads to a reduction in the flutter speed. Therefore the flutter characteristics of the deformed wing are shown to be very different, the critical speed lowers with deflection, than that for an undeflected straight wing; thus, the effect of geometric nonlinearities cannot be neglected. These results, obtained in a different manner, show the same characteristics as Ref (5).

The responses of the deformed wing to '1 – Cosine' gust loads at various gust lengths and airspeeds, above and below the flutter speed, are presented in Figs 12 and 13. Exactly the same characteristics are found as with the modelling based upon the undeflected modes, notably that the geometric stiffening reduces the tip deflections, but there are significant differences in the response magnitudes, due to the effect of the structural coupling and also that as the flutter speed lowers with deflection, then the speed at which LCO commence also lowers.

6.0 DISCUSSION AND CONCLUSIONS

A combined modal/FE method has been coupled with the doublet lattice unsteady aerodynamics to produce a reduced order model for the prediction of static aeroelastic deflection, gust response and limit cycle oscillation behaviour. The approach has been demonstrated upon a flexible high aspect ratio wing with varying structural properties and the results are encouraging. The inclusion of a nonlinear geometric stiffening behaviour is beneficial in resisting gust response compared to the linear case. The static and dynamic aeroelastic predictions have similar characteristics to those found by other researchers, but as there is no stall model included in the aerodynamics, it is not possible to make a direct comparison.

Although the approach has only been applied to a simplistic wing, the methodology is directly applicable to real wings as long as the dynamic behaviour can be broken down into a simple modal description (i.e. bending/torsion/edgewise bending) including coupling of these modes. The extension of the methodology to the free-free case will not be straightforward, but the way forward can be seen. The addition of the above nonlinear wing modelling approach to a free-free aircraft model is not so difficult, resulting in a combination of rigid body and flexible modes. However, one aspect not yet considered is the nonlinear inertia behaviour, and this will need to be considered in future models, including nonlinear inertia terms.

Research is continuing to develop the theoretical approach to include the nonlinear inertia terms, stall model aerodynamics and to also apply it to free-free aircraft models. An experimental evaluation of the approach is also planned in the near future.

ACKNOWLEDGEMENTS

The authors wish to thank to the Malaysian Ministry of Higher Education (MOHE) and the Universiti Putra Malaysia (UPM) for their support of M.Y. Harmin in this work. They are grateful for the input of Dr Gareth Vio, University of Sydney, and Dr Hamed Haddad Khodaparast, Dr Marco Prandina and Dr Wang Weizhuo of the Dynamics & Control Group at the University of Liverpool for useful discussions and assistance.

REFERENCES

1. NOLL, T.E., BROWN, J.M., PEREZ-DAVIS, M.E., ISHMAEL, S.D., TIFFANY, G.C. and GAIER, M. Investigation of the Helios prototype aircraft mishap, 2004, Vol I, *Mishap Report*.
2. PALACIOS, R., CESNIK, C.E.S. and REICHENBACH, E.Y. Re-examined structural design procedures for very flexible aircraft, *Engineering Analysis*, 2007, pp 1-19.
3. PALACIOS, R. and CESNIK, C.E.S. Structural models for flight dynamic analysis of very flexible aircraft, *Daedalus Boston*, May 2009, pp 1-17.
4. PATIL, M. and HODGES, D.H. On the importance of aerodynamic and structural geometrical nonlinearities in aeroelastic behavior of high-aspect-ratio wings, *J Fluids and Structures*, August 2004, **19**, (7), pp 905-915.
5. PATIL, M., HODGES, D.H. and CESNIK, C.E.S. Limit-cycle oscillations in high-aspect-ratio wings, *J Fluids and Structures*, January 2001, **15**, (1), pp 107-132.
6. PATIL, M.J., CESNIK, C.E.S. and HODGES, D.H. Nonlinear aeroelastic analysis of complete aircraft in subsonic flow, *J Aircr*, 2000, **37**, (5), pp 753-760.
7. SHEARER, C.M. and CESNIK, C.E.S. Nonlinear flight dynamics of very flexible aircraft, *J Aircr*, 2007, **44**, (5), pp 1528-1545.
8. CESNIK, C.E.S., SU, W. and FELLOW, A. Nonlinear aeroelastic modeling and analysis of fully flexible aircraft, April 2005, AIAA-2005-2169, 46th AIAA/ASME/ASCE/AHS/ASC Structures, Structural Dynamics and Materials Conference, Austin, TX, USA, pp AIAA-2005-2169.
9. WANG, Z., CHEN, P.C., LIU, D.D., MOOK, D.T. and PATIL, M.J. Time domain nonlinear aeroelastic analysis for HALE wings, 2006, 47th AIAA/ASME/ASCE/AHS/ASC Structures, Structural Dynamics and Materials Conference: 14th AIAA/ASME/AHS Adaptive Structures Conference, Eighth AIAA Non-deterministic App, **5**, pp 488-506.
10. MCEWAN, M.I., WRIGHT, J.R., COOPER, J.E. and LEUNG, A.Y.T. A finite element/modal technique for nonlinear plate and stiffened panel response prediction, 2001, 42nd AIAA/ASME/ASCE/AHS/ASC Structures, Structural Dynamics and Materials Conference and Exhibit Technical Papers, **1**, pp 3061-3070.
11. MCEWAN, M.I., WRIGHT, J.R., COOPER, J.E. and LEUNG, A.Y.T. A combined modal/finite element analysis technique for the dynamic response of a non-linear beam to harmonic excitation, *J Sound and Vibration*, 2001, **243**, (4), pp 601-624.
12. RADU, A.G., YANG, B., KIM, K. and MIGNOLET, M.P. Prediction of the dynamic response and fatigue life of panels subjected to thermo-acoustic loading, 2004, 45th AIAA/ASME/ASCE/AHS/ASC Struct Dyn and Mater Conf; 12th AIAA/ASME/AHS Adapt Struct Conf; 6th AIAA Non-Deterministic Approaches Forum; Fifth AIAA Gossamer Spacecraft Forum, **1**, pp 520-528.
13. MURAVYOV, A. and RIZZI, S.A. Determination of nonlinear stiffness with application to random vibration of geometrically nonlinear structures, *Computers & Structures*, July 2003, **81**, (15), pp 1513-1523.
14. HOLLKAMP, J.J., BEBERNISS, T.J. and GORDON, R.W. The nonlinear response of a plate to acoustic loading: predictions and experiments, 2006, 47th AIAA/ASME/ASCE/AHS/ASC Structures, Structural Dynamics and Materials Conference, 14th AIAA/ASME/AHS Adaptive Structures Conference, Eighth AIAA Non-deterministic App, **6**, pp 4047-4063.
15. LIU, D.D., WANG, Z., YANG, S., CAI, C., WANG, X.Q. and MIGNOLET, M.P. Nonlinear aeroelastic methodology for a membrane-on-ballute model with hypersonic bow shock, 2009, 50th AIAA/ASME/ASCE/AHS/ASC Structures, Structural Dynamics and Materials Conference.
16. SCOTT, R.C., BARTELS, R.E. and KANDIL, O.A. An aeroelastic analysis of a thin flexible membrane, 2007, 48th AIAA/ASME/ASCE/AHS/ASC Structures, Structural Dynamics and Materials Conference, **8**, pp 7459-7475.
17. RODDEN, W. and JOHNSON, E. *MSC/NASTRAN Aeroelastic Analysis User's Guide*, 1994, MSC.
18. HARMIN, M.Y. and COOPER, J.E. Dynamic aeroelastic prediction for geometrically nonlinear aircraft, 2011, International Forum of Aeroelasticity and Structural Dynamics, pp IFASD-2011-050.
19. WRIGHT, J.R. and COOPER, J.E. *Introduction to Aircraft Aeroelasticity and Loads*, 2008 Aerospace Series (PEP)), p 524, Wiley.
20. ROGER, K.L. Airplane math modeling methods for active control design, 1977, *AGARD*, 228, p 11.
21. *ZAERO Theoretical Manual*, Version 8.4, 20th edition, 2008, ZONA Technology, Scottsdale, AZ, USA.

https://doi.org/10.1017/S0001924000006515 Published online by Cambridge University Press

3RD AIRCRAFT STRUCTURAL DESIGN CONFERENCE

CONFERENCE TOPICS

DELFT UNIVERSITY, THE NETHERLANDS/ 9-11 OCTOBER 2011

Structural designs for the next generation of aircraft

- To meet the environmental challenges
- To meet high volume traffic requirements
- To meet high volume manufacturing requirements
- To meet cost and requirement constraints
- To meet emerging requirements for improved safety and crash worthiness
- To reduce time to market

Design with novel or advanced materials

- Innovative use of CRFP including aeroelastic tailoring
- Re-cycling and re-use of CRFP
- CRFP structural design for maintenance and repair
- Role of GLARE and other fibre-metal laminates (CentrA1, TiGrE, etc)
- Role for advanced metal alloys
- Novel materials
- Manufacturing with novel materials
- Certification of novel materials

For further information please visit www.aerosociety.com/events

ORGANISING COMMITTEE

Chairman
Prof Alan Morris, FReng, RAeS, UK

Local Organising Committee
Prof Zafer Gurdal, Delft University, NL-Chairman
Prof Michael van Tooren, Delft University, NL
Prof Rinze Benediktus, Delft University, NL
Mr Christos Kassapoglou, Delft University, NL
Dr Rene Alderliesten, Delft University, NL
Dr Gianfranco La Rocca, Delft University, NL

International Organising Committee
Paul Arendsen, NLR, Netherlands
Prof Horst Baier, Inst of Lightweight Structures, Germany
Prof Chiara Bisagni, Politecnico di Milano, IT
Prof Carlos Cesnik, University of Michigan, USA
Prof Jonathan Cooper, University of Liverpool, UK
Dr Kota Harinarayana, India
Prof Andy Keane, University of Southampton, UK
Yiu-Wing Mai, University of Sydney, Australia
Prof Joaqium Martins, University of Michigan, USA
Dr Adrian Murphy, Queen's University Belfast, UK
Dr Malcolm Nash, RAeS, UK
Prof Constantinos Soutis, University of Sheffield, UK
Dr Martin Spieck, DLR Deutsches Zentrum fur Luft-und Raumfahr, Germany
Prof Afzal Suleman, University of Victoria, CA
Prof Vassili Toropov, University of Leeds, UK
Prof Rade Vignevic, Cranfield University, UK
Prof Paul Weaver, University of Bristol, UK
Prof Karen Willcox, MIT, USA
Prof Zheng Zhong, Tonjii University, Shanghai, China

KEY DATES AND DEADLINES
Abstracts submitted by: 26 March 2012

https://doi.org/10.1017/S0001924000006515 Published online by Cambridge University Press

CONFERENCE AND EVENTS DEPARTMENT
Royal Aeronautical Society